Journal of Quantitative Spectroscopy & Radiative Transfer 243 (2020) 106800

Contents lists available at ScienceDirect

Journal of Quantitative Spectroscopy & Radiative Transfer

journal homepage: www.elsevier.com/locate/jqsrt

Impact of δ-Four-Stream Radiative Transfer Scheme on global climate model simulation

Quan Yang[a], Feng Zhang[a,b,*], Hua Zhang[b], Zhili Wang[b], Hironobu Iwabuchi[c], Jiangnan Li[d]

[a] Key Laboratory of Meteorological Disaster, Ministry of Education/Joint International Research Laboratory of Climate and Environment Change/Collaborative Innovation Center on Forecast and Evaluation of Meteorological Disaster, Nanjing University of Information Science & Technology, Nanjing 210044, China
[b] State Key Laboratory of Severe Weather, Chinese Academy of Meteorological Sciences, Beijing 100081, China
[c] Center for Atmospheric and Oceanic Studies, Tohoku University, Sendai, Miyagi 980-8577, Japan
[d] Canadian Center for Climate Modeling and Analysis, University of Victoria, British Columbia 999040, Canada

ARTICLE INFO

Article history:
Received 17 August 2019
Revised 2 December 2019
Accepted 13 December 2019
Available online 14 December 2019

Keywords:
Radiative transfer scheme
δ-4DDA
Global climate model

ABSTRACT

The impact of radiative transfer scheme on global climate model (GCM) simulation is presented in this paper by comparing the difference between δ-two-stream adding method (δ-2DDA) and adding algorithm of the δ-four-stream discrete ordinates method (δ-4DDA) radiation schemes in the Atmospheric General Circulation Model of the Beijing Climate Center (BCC_AGCM). Only consider the effects of the calculation method itself, the δ-4DDA reduces the negative shortwave cloud radiative effect (CRE) in the areas with a significant fraction of low cloud, while enhances the negative shortwave CRE in the areas with the large fraction of high cloud. For the longwave CRE, the δ-4DDA enhances the longwave CRE drastically in the regions with a significant fraction of the high cloud. The feedback of clouds results in more interesting results. The δ-4DDA produces more accurate shortwave CRE in the region over the land and ocean in the middle and high latitude areas. The longwave CRE simulated by δ-4DDA is better than that affected by δ-2DDA over the ground in Africa, South America, and Atlantic. The change of radiation scheme affects the simulation of other meteorological variables. The simulation of global humidity by δ-4DDA is improved obviously. The δ-4DDA simulates more accurate temperature in continents of the northern hemisphere and precipitation in North America, Africa, northern Indian Ocean and western Pacific. Although the improvement of every physical process is required to develop the models, implementing δ-4DDA scheme into GCM and evaluating the effect of it are necessary and meaningful.

1. Introduction

Global climate models are the primary tool used for climate change projections. The uncertainty of the parameterization schemes in the global climate model limits the accuracy of future climate change projections. Radiation process is one of the most crucial factors for climate modeling, affecting the simulation result of climate to a large extent.

The radiative transfer algorithm is pivotal for radiative processes in climate models. Over the past few decades, numerous works have been done to obtain a more straightforward method to parameterize the radiative processes with higher accuracy (e.g., [9,13,15,20,24,26,29,34,44,47,48,54,57,58]). The δ-two-stream methods, which provide a simple calculative process and moderately accurate analytical solutions of the radiative transfer equation, are the most common choice in climate models among other available methods [39]. However, cloud heating was underestimated as high as 10% by δ-two-stream methods [34]. The incorrect cloud absorption could affect climate model behaviors as cloud top heating is crucial for cloud evolution, which indicates that a δ-four-stream scheme is necessary. Liou et al. [30] derived the solution of the δ-four-stream discrete ordinates method (DOM) for a single layer atmosphere. The δ-four-stream DOM was extended to a vertically inhomogeneous atmosphere by using an inverse matrix formulation to solve the connection of all the layers in radiative transfer [15]. Using a combination of the δ-four stream DOM for solar radiation and δ-two-and-four-stream DOM for thermal infrared radiation in a climate model, Gu et al. [16] found that the use of the new radiation scheme improved the model simulated cloud and radiation fields and alleviated the cold bias that is common in many climate models.

The adding method works naturally with layered medium and yields reflection and transmission readily. Besides, the advantage of the adding method is that the calculation is performed one layer

* Corresponding author.
E-mail address: fengzhang@nuist.edu.cn (F. Zhang).

https://doi.org/10.1016/j.jqsrt.2019.106800
0022-4073/

at a time, without the requirement for handling the inverse of a large matrix associated with all the model layers. Another advantage of the adding method is its ability to manage partial cloud under a specific condition [27] since dealing with vertical overlap and internal inhomogeneity of cloud is a challenging task in atmospheric radiation. Because of these advantages, the δ-two-stream adding method (referred as δ-2DDA) [2,3,25,50,55] is widely used in climate models. Zhang et al. [57] created an adding algorithm of the δ-four-stream DOM (referred to as δ-4DDA) for solar radiation. The δ-4DDA scheme was applied to improve the calculation accuracy of aerosol radiation forcing [65]. Zhang et al. [59] proposed an infrared δ-4DDA based on the invariance principle. The δ-4DDA method is much more accurate than δ-2DDA method in most cases, especially under the cloudy-sky condition. Besides, the δ-4DDA method is much more efficient than δ-four-stream DOM [28]. The computational time of the δ-4DDA is about 1.76 times of that of δ-2DDA for a radiative transfer calculation with gaseous transmission and cloud absorption [28]. Therefore, the current computers can manage the extra computation very well in climate modeling. It is necessary to assess the impact of δ-4DDA on global climate models (GCMs).

In GCM, the heating and cooling rates obtained by radiative transfer calculations would involve the calculation of the thermal process, which further alters the dynamic processes [31,49]. Different radiation transfer algorithms will inevitably lead to different simulation results. The δ-4DDA scheme for solar and infrared radiation have not been combined for systematic analysis and assessment in climate models. In this study, the simulation results of δ-4DDA and δ-2DDA on radiation variables and other meteorological variables will be evaluated in the GCM.

The model and the data are introduced briefly in Section 2. Section 3 presents the results of the fluxes, cloud radiative effect and meteorological variables simulated by δ-4DDA and δ-2DDA schemes in a GCM. A conclusion and discussion are given in Section 4.

2. Model and data

2.1. Model description

In this study, the Atmospheric General Circulation Model of the Beijing Climate Center (BCC_AGCM2.0.1) is used to estimate the impact of different radiative transfer schemes. The BCC_AGCM2.0.1 is developed from the Community Atmosphere Model Version 3 (CAM3) of the National Center for Atmospheric Research (NCAR) [53]. The model employs horizontal triangular truncation at wavenumber 42 (T42, approximately 2.8° × 2.8°) and a terrain-following hybrid vertical coordinate including 26 layers with the top layer at a pressure of 2.9hPa.

Some improvements have been implemented in the cloud-radiative processes in BCC_AGCM2.0.1. To make the representation of subgrid cloud properties flexible and modularized and to maintain computational efficiency, the Monte Carlo Independent Column Approximation (McICA) method is used [18,40]. A stochastic sub-grid cloud generator combined with McICA developed by Jing and Zhang [21] is adopted in the cloud overlap scheme to solve the problem of subgrid cloud variability. The radiative parameterization employed is the Beijing Climate Center Radiation transfer model (BCC_RAD), which was developed by Zhang et al. [60–62]. In the BCC_RAD, the radiation spectrum is divided into 17 bands (eight bands for longwave and nine bands for shortwave), and the spectral ranges of each band are listed in Zhang et al. [60]. The model contains five major greenhouse gasses (H_2O, CO_2, O_3, N_2O, and CH_4) and chlorofluorocarbons (CFC11, CFC12, CCL4, and CFC22). The optical properties of water cloud droplets are taken from Nakajima et al. [38] and Kiehl et al. [23], respectively. The optical properties of ice clouds are computed using data from Zhang et al. [64]. More details of BCC_RAD can be found in Zhang et al. [63]

The δ-2DDA and δ-4DDA are used to deal with the solar and thermal radiation transfer calculation in BCC_RAD. In solar and infrared δ-4DDA, the four-stream discrete ordinates method [30,31] with two-node Gaussian quadrature ($\mu_1 = 0.2113$, $\mu_2 = 0.7887$) is used to solve the radiation equation in a single layer. The four principles of invariance governing the reflection and transmission of the light beam for solar radiative transfer proposed by Chandrasekhar [5] and for infrared radiative transfer proposed by Zhang et al. [59] are the basis of the adding mothed, which can be applied to multilayer atmospheric radiation transmission.

2.2. Data and methodology

The primary datasets used in this article comes from model simulations. Two experiments are designed to reveal the differ-

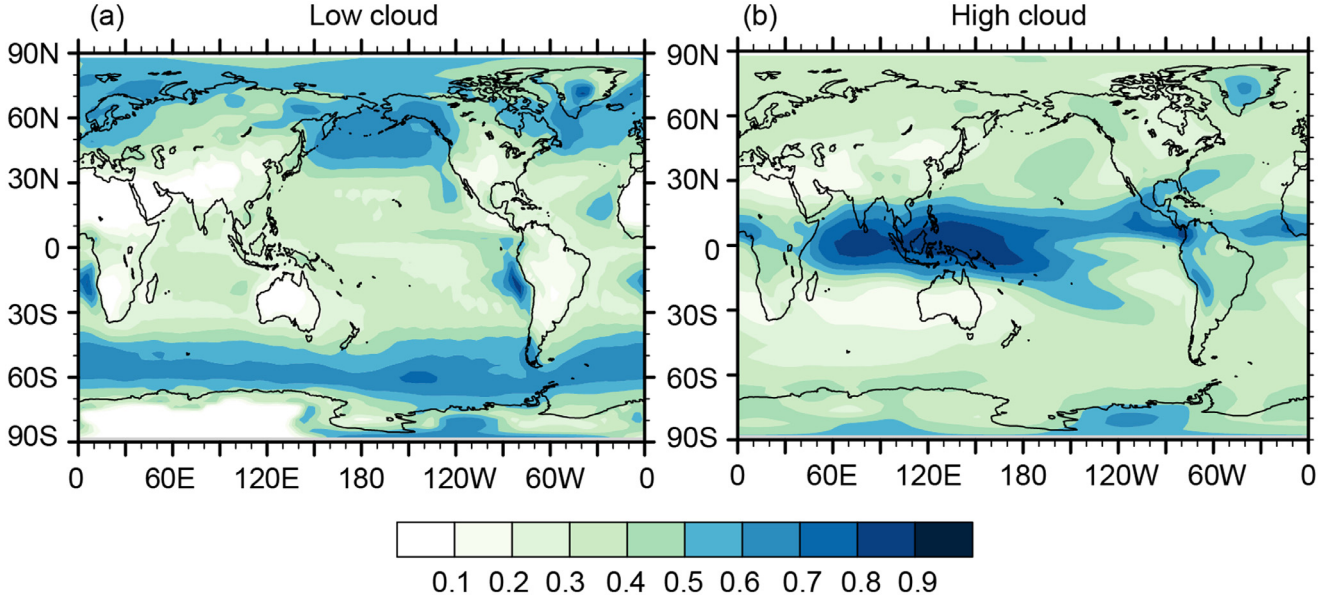

Fig. 1. Global distributions of the cloud fraction in instantaneous diagnose experiment.

ences between the two kinds of radiative transfer schemes in GCM. In the first instantaneous diagnose experiment, the δ-2DDA and δ-4DDA are used as the first and second calculations, respectively. In the model integrations, the model fields are only updated using the radiative results from the δ-2DDA. Therefore, there was no climate feedback from the δ-4DDA. In this instantaneous diagnose experiment, the cloud properties and meteorological variables are the same for the δ-2DDA and δ-4DDA. In the second experiment, both the δ-2DDA and δ-4DDA are used to drive the model respectively, to obtain the different status of cloud and meteorological variables, which is referred to as the feedback experiment. The prescribed present SST and the sea ice data are adopted in these two experiments. The model runs from 1975 to 2010, and the monthly average output results of 1981–2010 are used for analysis.

The monthly fluxes and cloud radiative effect (CRE) datasets from 2.8 Edition Energy Balanced and Filled (EBAF) are provided by the Clouds and the Earth's Radiant Energy System (CERES). The data for monthly surface temperature, specific humidity, and relative humidity come from the National Centers for Environmental Prediction (NCEP) and the National Center for Atmospheric Research (NCAR). The monthly precipitation data come from the Global Precipitation Climatology Project (GPCP) Version 2.3 Combined Precipitation Data Set. The 30-year averages of these data from 1981 to 2010 are used as benchmarks to evaluate the simulation results of the δ-2DDA and δ-4DDA in GCM.

3. Comparisons in GCM

3.1. Instantaneous diagnose experiment

In the instantaneous diagnose experiment, meteorological variables are consistent, and only the radiation variables calculated in the radiation process will change. Clouds affect the radiation budget of the Earth through their interaction with shortwave (solar) and longwave (thermal) radiation. On the one hand, some amount of the incoming shortwave radiation is reflected and absorbed by clouds; on the other hand, clouds absorb the longwave radiation emitted by Earth, and in turn, re-emit longwave radiation back to the Earth and space [43]. Therefore, clouds are one of the dominant modulators of the radiation budget at the top of the atmosphere (TOA) and the surface (SFC) [11,42,46]. In the instantaneous diagnose experiment, the cloud fraction is the same. In BCC_AGCM, clouds at pressures greater than 680hPa are defined as low clouds, and clouds at pressures less than 440hPa are defined as a high cloud. Fig. 1 presents the distribution of low (Fig. 1a) and high (Fig. 1b) clouds in this experiment. For the low cloud, the areas of the large fraction are located in high latitudes in the northern hemisphere (60° – 90°N), and the high-value belt in the southern hemisphere is located in mid-latitudes (40° – 70°S). At the same latitude, the fraction of low cloud over the land lower than that over the ocean, which is consistent with observations [12]. For the high cloud, large values of the fraction are concentrated over the ocean near the equator, especially in the western Pacific and Indian

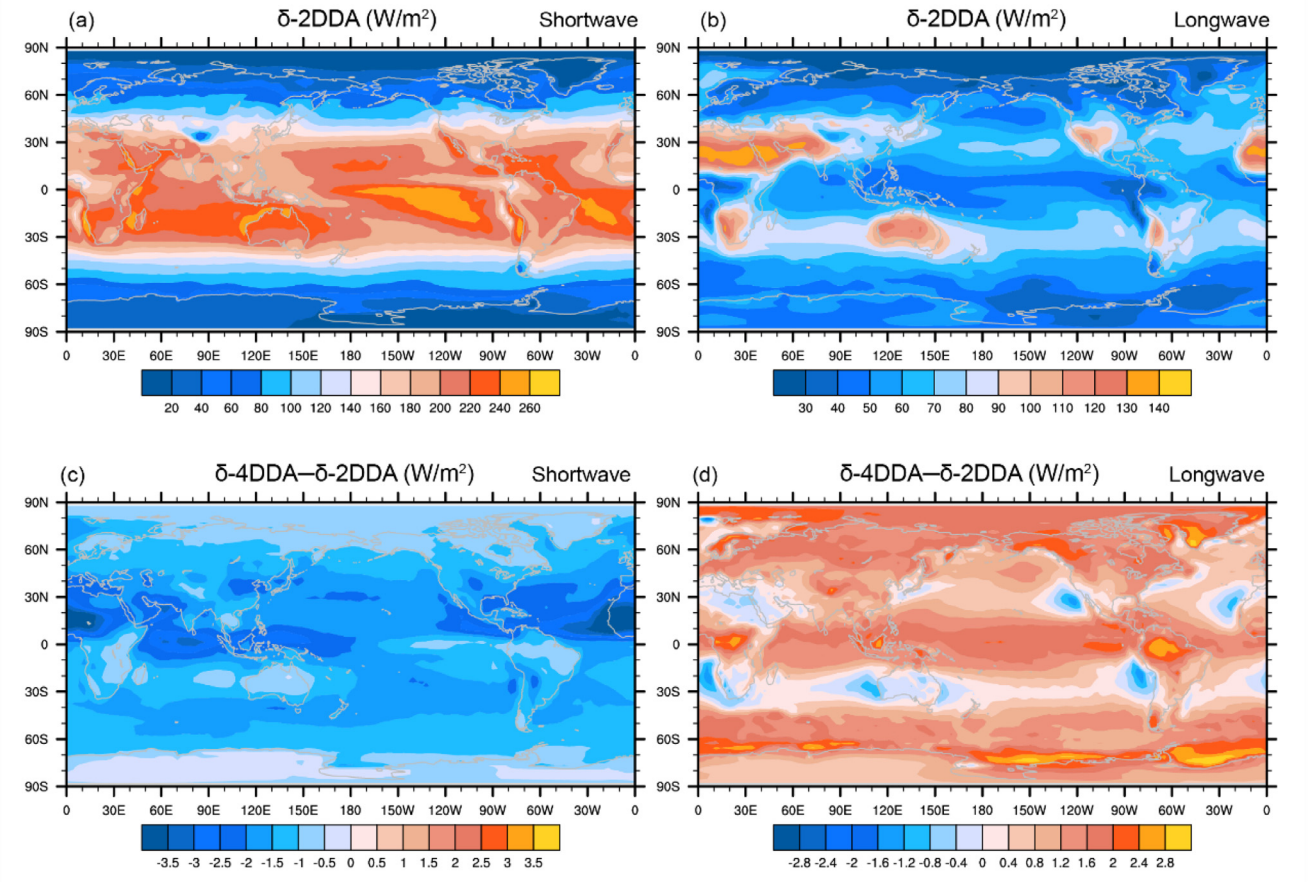

Fig. 2. Global distributions of (a) (b) net flux at SFC simulated by δ-2DDA, and (c) (d) differences between two schemes for (a) (c) shortwave and (b) (d) longwave in instantaneous diagnose experiment.

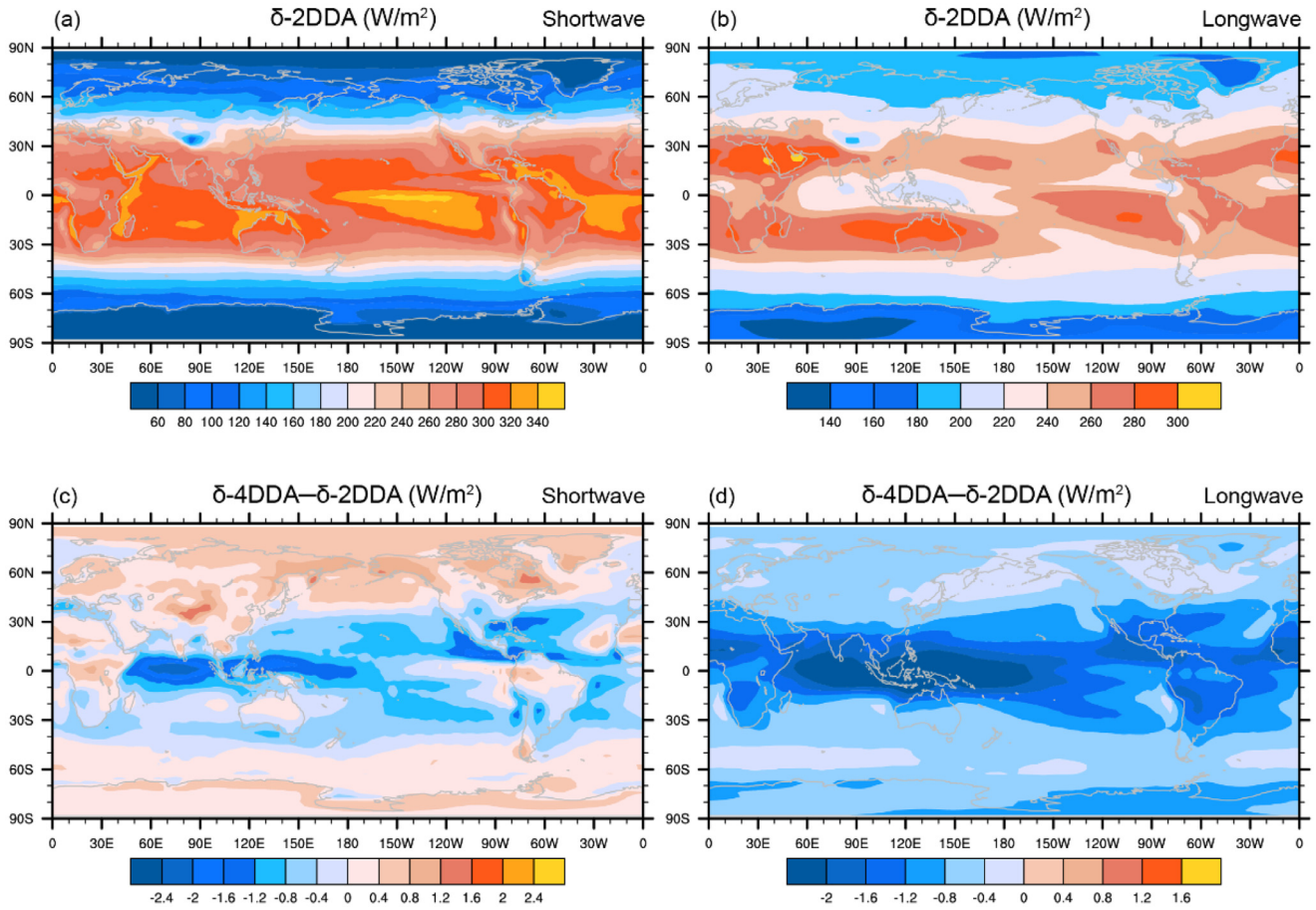

Fig. 3. Same as Fig. 2, but the net flux at TOA.

Ocean warm pool regions. In tropics, the updraft is very strong, leading to more high clouds and less low clouds.

The δ-4DDA scheme has a higher-order approximation than the δ-2DDA. Theoretically, the higher the order, the more accurate the calculation. To verify the accuracy of the two schemes, both of the two schemes are incorporated to BCC_AGCM to calculate the radiation flux for a group of the instantaneous diagnose experiment. Shortwave and longwave net flux at the SFC simulated by δ-2DDA and the difference between δ-4DDA and δ-2DDA are shown in Fig. 2. If the absorption and reflection of clouds and gases are ignored, the shortwave net flux at SFC will decrease with increasing latitude. Due to the extinction of cloud on shortwave radiation, the SFC shortwave net flux near the Indo-Pacific Warm Pool and the Bering sea is significantly lower than that in the same latitude area. The shortwave net flux at SFC simulated by δ-4DDA is smaller than that simulated by δ-2DDA, and the global average difference is -1.37 W/m^2. The most significant difference occurred in the Sahara desert, with a value of -5.0 W/m^2. The cloud optical thickness is very small over the Sahara desert (Minnis et al., 2003 [36]). According to Zhang and Li, the transmittance of the δ-4DDA is significantly lower than that of the δ-2DDA when the optical depth is small [58], so the shortwave net flux at SFC simulated by δ-4DDA is significantly lower than that simulated by δ-2DDA in the Sahara desert. The difference between shortwave net fluxes at SFC simulated by the two schemes is more significant in areas with more high clouds, such as the Indo-Pacific Warm Pool. The shortwave net fluxes at SFC in regions with the fraction of high clouds greater than 0.5 and areas with the fraction of low clouds greater than 0.5 were calculated, respectively. In areas dominated by high clouds, the average difference in surface shortwave net flux is -1.7 W/m^2, while in areas dominated by low clouds, it was -1.1 W/m^2.

The longwave net flux simulated by δ-2DDA has a high value in the Sahara desert, the Arabian desert, the Australian desert, and the North American desert. These desert areas have less cloud cover, so the longwave net flux is large. The difference of the global average surface longwave net flux simulated by δ-4DDA and δ-2DDA is 1.12 W/m^2, and the longwave net flux simulated by δ-4DDA in most regions is higher than that simulated by δ-2DDA. According to Zhang et al. [59], in the standalone radiation model, the downward flux at SFC simulated by δ-4DDA is smaller in the presence of clouds, which is consistent with the results in this paper.

Similar to the shortwave net flux at SFC, the shortwave net flux at TOA near the Indo-Pacific Warm Pool is less than that in other regions at the same latitude due to the reflection of clouds (Fig. 3). The results of Zhang and Li [58] show that when the optical thickness is small, the reflectivity of δ-4DDA is larger than that of δ-2DDA; when the optical depth is large, the reflectivity of δ-4DDA is lower than that of $\delta-$2DDA. Therefore, the distribution of the difference in shortwave net flux at TOA simulated by the two schemes is not uniform. In the low-latitude ocean, the differences are mostly negative, with the most significant difference being -2.34 W/m^2 in the Indo-Pacific Warm Pool. While in the middle and high latitudes, the shortwave net flux simulated by δ-4DDA is larger than that of δ-2DDA. The average difference in shortwave net flux at TOA is -0.57 W/m^2 in the region dominated by high clouds, while in areas dominated by low clouds, the difference was 0.33 W/m^2.

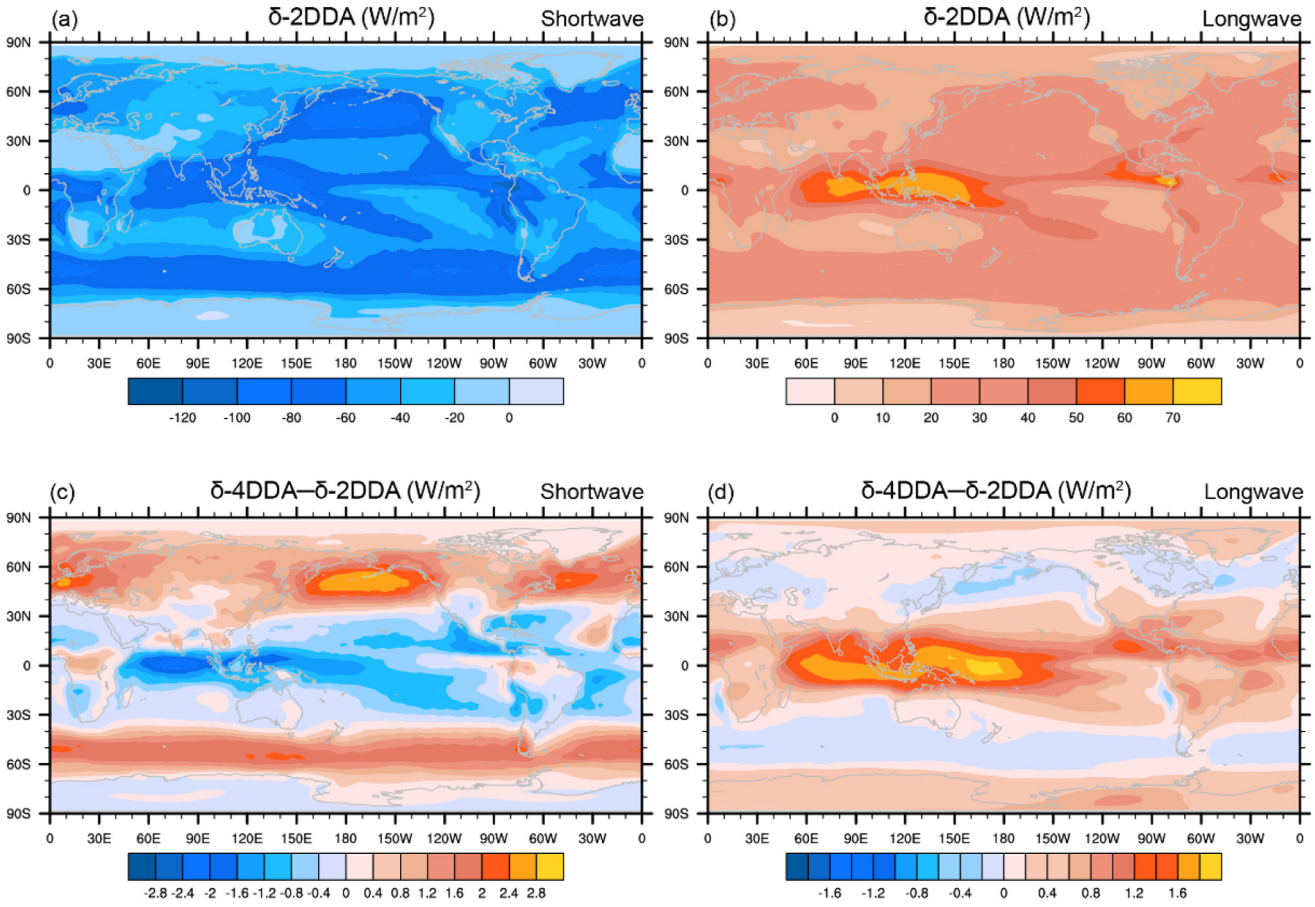

Fig. 4. Same as Fig. 1, but the CREs at TOA.

The longwave net flux at TOA determined by the upward emission of the surface and clouds is closely related to the temperature of the surface and the temperature of the cloud top. The simulation results of δ-2DDA decrease with the increasing latitude, but in the areas dominated by high clouds, the longwave net flux is significantly lower. δ-4DDA simulates lower longwave net flux at TOA than δ-2DDA, with a global average difference of -0.85 W/m^2 and a maximum difference of -2.48 W/m^2. The difference is more significant in the areas with high clouds than that with low clouds. In areas with high clouds fraction greater than 0.5, the difference between the two schemes is -1.56 W/m^2, while in areas with low clouds fraction greater than 0.5, the difference between the two schemes is -0.5 W/m^2.

In GCM, radiative effect (CRE) is a critical element causing the uncertainty [6,7,45,51]. CRE is defined by Ramanathan et al. [41] as the difference between cloudy and clear-sky radiation fluxes. As one of the essential indicators of the cloud effect on radiation, CRE has been widely used to assess the significance of clouds on radiation. Fig. 4 presents the CREs simulated by these two schemes in BCC_AGCM2.0.1 for the instantaneous diagnose experiment. Upper panels provide the CREs simulated by δ-2DDA. The bottom groups show the differences in the CREs simulated by δ-4DDA and δ-2DDA with the same cloud properties and other meteorological variables. The value of shortwave CRE at the TOA is negative (cooling effect). As the value of shortwave CRE at the TOA is negative, the negative difference in which between δ-4DDA and δ-4DDA means the enhancement or overestimation of the shortwave CRE. Also, the positive difference implies the reduction or underestimation of the shortwave CRE. The δ-4DDA reduces the CREs over the land and sea in the middle and high latitudes with a significant fraction of low clouds, such as the Bering Strait region and the ocean region around 60° south. The maximum reduction is more than 2.8 W/m^2. In the areas with a large fraction of high cloud, the δ-4DDA enhances the negative shortwave CRE. Especially for the region of the Indian Ocean warm pool, the δ-4DDA enhances the negative shortwave CRE, with the maximum absolute value exceeding 2.4 W/m^2. The global distributions of the longwave CRE at the TOA simulated by δ-2DDA and differences of the two schemes are presented in the right panels. Compared with the δ-2DDA, δ-4DDA enhances the longwave CRE in most areas (Fig. 4d). The differences of longwave CREs between the δ-4DDA and δ-2DDA are related to the high cloud. In the areas with a large fraction of the high cloud, the δ-4DDA enhances the longwave CRE drastically. The most considerable enhancement is in the western Pacific Ocean, exceeding 2.0 W/m^2.

3.2. Feedback experiment

The change of fluxes caused by the different calculation schemes creates an interaction effect with clouds. In the instantaneous diagnose experiment, only the impact of the method itself is considered. In a feedback experiment, the interaction of cloud-radiation is taken into account. Fig. 5 presents the distributions of the differences in cloud fraction between the δ-2DDA and δ-4DDA schemes. The distributions of the low and high cloud fraction simulated by the δ-2DDA are shown in Fig. 1. The fraction of the low cloud simulated by the δ-4DDA is higher than that simulated by δ-2DDA over large regions, with a global average difference of 0.0075 (Fig. 5a). The δ-4DDA enhances the fraction of the high cloud that appeared in the land near the equator, especially

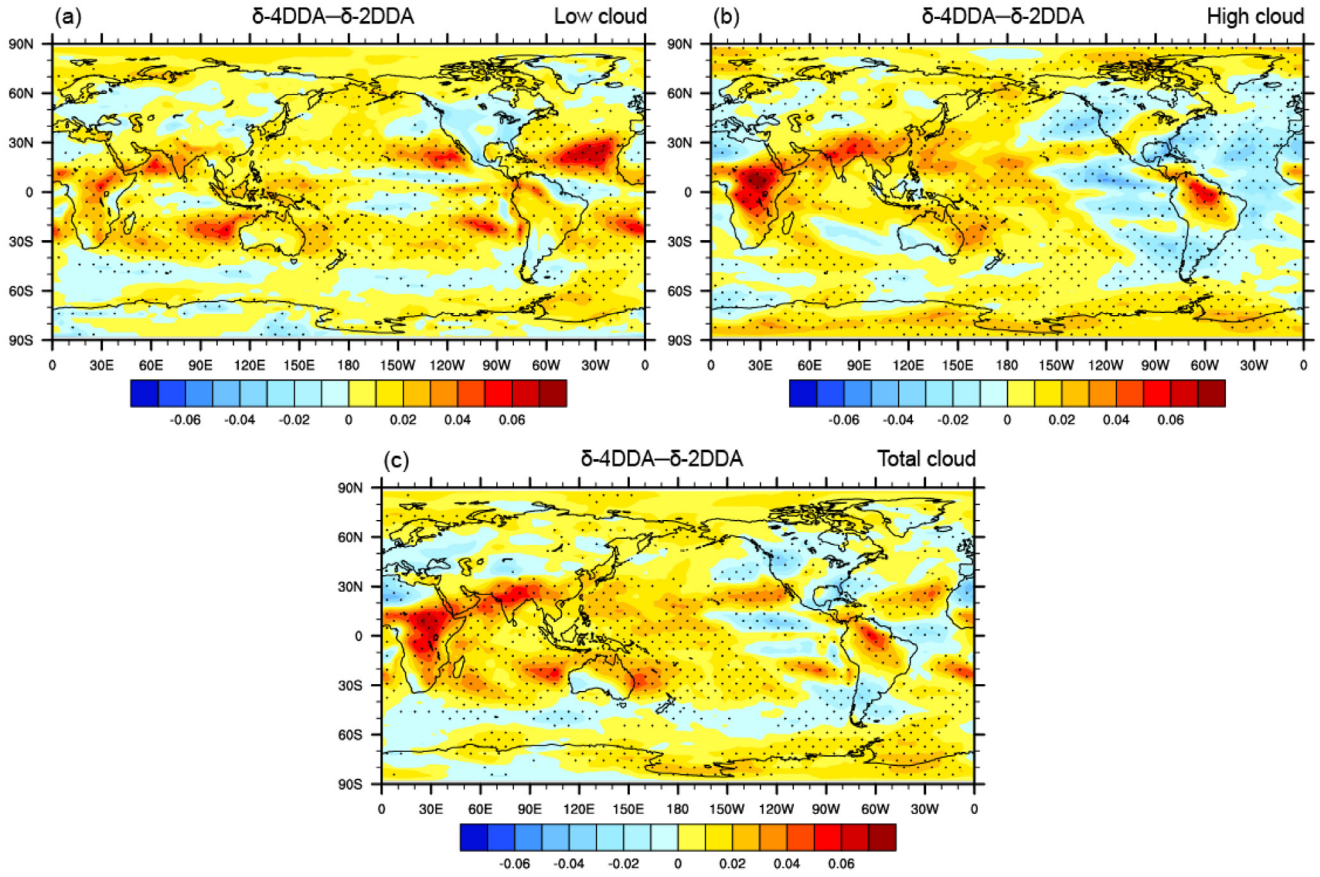

Fig. 5. Global distributions of the differences between two schemes for (a) low cloud, (b) high cloud and (c) total cloud in the feedback experiment. The black dots indicate where differences exceeded the 90% confidence level.

in the center of Africa, with a maximum value of 0.082, while it reduces the fraction of the high cloud in the Atlantic and eastern Pacific (Fig. 5b). The δ-4DDA scheme overestimates the total cloud fraction over large regions, especially in the center of Africa and India. In some areas of the eastern Pacific and Europe, the δ-4DDA scheme underestimates the total cloud fraction compared to the δ-2DDA (Fig. 5c).

Because of the feedback of clouds, both the shortwave and longwave fluxes and CREs are different from those of the diagnosing experiment. Fig. 6 shows the difference between the shortwave (longwave) net flux at SFC simulated by δ-2DDA and the CERES data, as well as the difference between δ-4DDA and δ-2DDA in the feedback experiment. Compared with CERES, the shortwave net flux at SFC simulated by δ-2DDA on the continent in low latitude is higher, but the global averaged surface shortwave net flux is smaller, with an average value of -4.41 W/m^2. In the feedback experiment, the difference in shortwave net flux at SFC between the two schemes is more complicated due to the change of cloud fraction. In terms of quantity value, the difference in the feedback experiment was also more significant than that in the diagnostic experiment, with the maximum difference as high as -15.9 W/m^2. In the diagnostic experiment, shortwave net flux at SFC simulated by δ-4DDA is smaller than that simulated by δ-2DDA in the global area. While in the feedback experiment, the shortwave net flux of δ-4DDA in some areas are larger than that of δ-2DDA, because the cloud cover in these areas simulated by δ-4DDA is reduced, making more solar radiation reach the surface. At the same time, the surface shortwave net flux simulated by δ-4DDA is further reduced in the region with increased cloud fraction.

The global mean longwave net fluxat SFC simulated by δ-2DDA is higher than the CERES data, with the significantly higher value in China and India, and lower value in the Indo-Pacific Warm Pool. Compared with δ-2DDA, the longwave net flux at SFC simulated by δ-4DDA is lower in the regions with increased cloud fraction, such as central Africa, Arabian peninsula and India, because the increase of the cloud raises the surface downward longwave radiation. The decreased surface longwave net flux due to the change of cloud was of a larger magnitude, and the difference in the global mean surface longwave net flux between δ-4DDA and δ-2DDA changed from the positive value (1.12 W/m^2) in the diagnostic experiment to the negative value (-0.03 W/m^2) in feedback experiment.

Compared with CERES, δ-2DDA simulates a lower global mean shortwave net flux at TOA with an average value of -7.19 W/m^2. In the Sahara desert, east Asia, South America and Australia, δ-2DDA simulates a higher shortwave net flux at TOA than the CERES data. In the diagnostic experiment, the shortwave net flux at TOA in the mid-high latitude region simulated by $\delta-$4DDA is higher than that simulated by δ-2DDA. In the feedback experiment, some areas reflect more solar radiation due to the increase of cloud cover, making the δ-4DDA simulate lower shortwave net flux compared to δ-2DDA. Similarly, in the lower latitudes, the reduction of cloud cover over the western Pacific and Atlantic ocean makes the shortwave net flux at TOA simulated by the $\delta-$4DDA in this region higher than that simulated by δ-2DDA.

Compared with CERES, δ-2DDA overestimates the longwave net flux at TOA in Africa and South America with a maximum error of 41.41 W/m^2. However, δ-2DDA underestimates the longwave net flux at TOA in both the Indian Ocean and the western Pacific with a

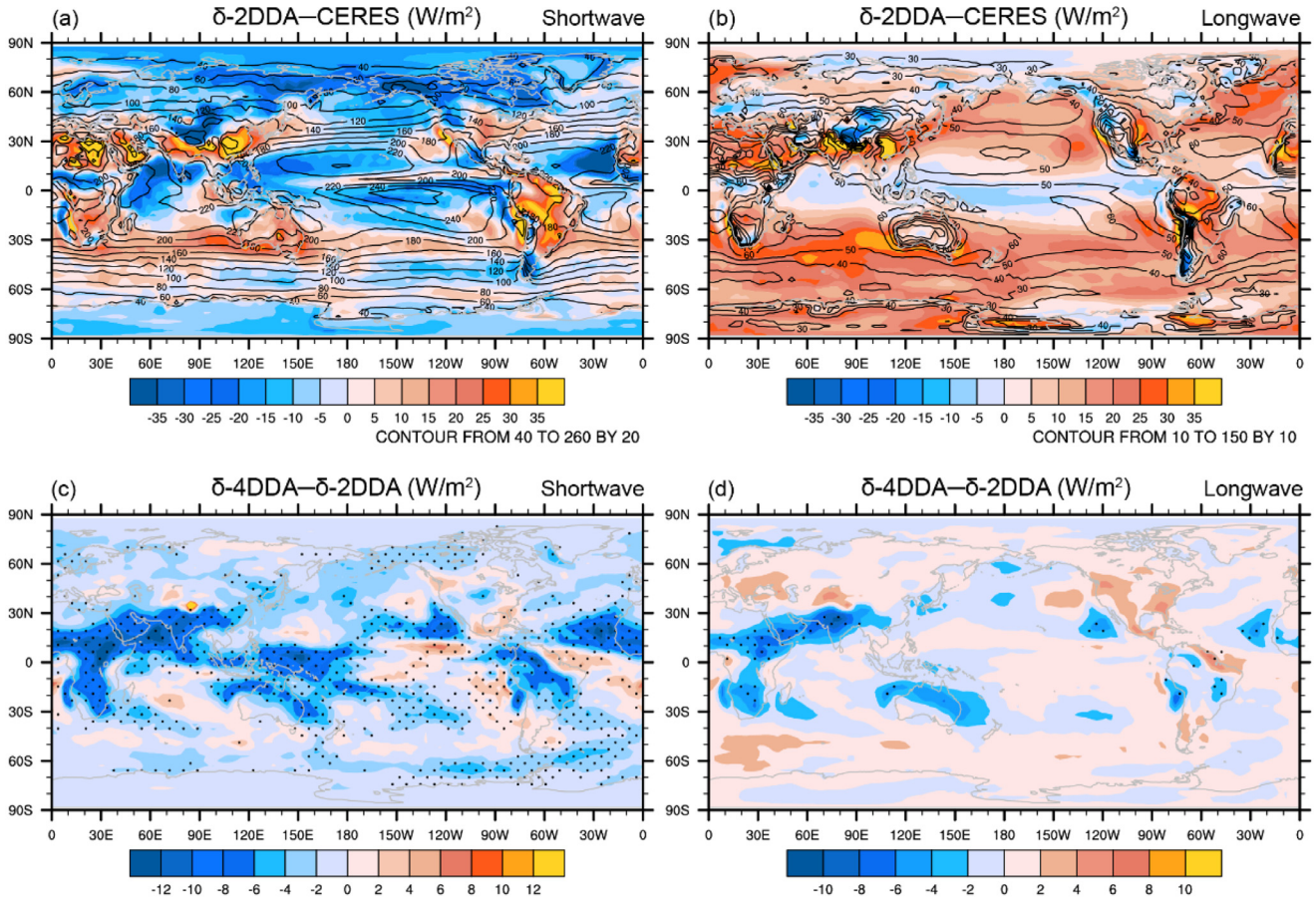

Fig. 6. Global distributions of (a) (b) differences in net fluxes at SFC between δ-2DDA and CERES, and (c) (d) differences between two schemes for (a) (c) shortwave and (b) (d) longwave in feedback experiment. The contours in (a) (b) are the net fluxes of CERES's observation.

maximum error of -32.61 W /m^2. In the feedback experiment, the longwave net flux at TOA is significantly affected by the change of high clouds. Because of the decrease in high clouds fraction simulated by δ-4DDA over Atlantic and western Pacific regions, the longwave net flux at TOA simulated by δ-4DDA in this region also changed from lower than that simulated by δ-2DDA in diagnostic experiments to higher than that simulated by δ-2DDA in feedback experiment (Fig. 7).

Upper panels of Fig. 8 provide the observed CREs at TOA from CERES data and the differences between δ-2DDA and the observed results; the bottom presents the distribution of differences in CREs simulated by the δ-4DDA and δ-2DDA in the feedback research. In the Sahara desert and Antarctica, CREs of CERES data is small, where there are fewer low clouds. However, the absolute values of shortwave CRE are significant for the ocean in mid-latitude. From Fig. 8a, the δ-2DDA overestimates the shortwave CRE in the areas over the ocean around the equator. The differences of shortwave CREs between the δ-2DDA and δ-4DDA schemes are related to the different total cloud fraction simulated in the GCM. The incoming shortwave radiation can be reflected and absorbed by clouds. The existence of clouds enhances the reflected shortwave fluxes at the TOA. In the areas around the center of Africa and India, the δ-4DDA enlarges the cooling effect compared with the δ-2DDA since the fraction of the total cloud is enhanced by the δ-4DDA observably. In the instantaneous diagnose experiment, the δ-4DDA also enlarges the cooling effect in the eastern Pacific. However, the δ-4DDA reduces the cooling effect in some areas over the eastern Pacific in feedback experiment because of the decrease of the total cloud fraction simulated by it. Over the middle and high latitudes, though the fraction of whole cloud simulated by the δ-4DDA is larger than that simulated by δ-2DDA, the δ-4DDA doesn't enlarge the cooling effect in these areas. In these areas, the δ-4DDA underestimates the negative CRE compared to the δ-2DDA according to the instantaneous diagnose experiment. Therefore, in the feedback experiment, the cooling effect of the increased cloud fraction is offset by the warming impact of the calculation method.

In the warm pool regions of the Indian and western Pacific oceans, the values of CERES longwave CREs are largest. And then in the equatorial continent, the longwave CREs are also larger. Over the land, the δ-2DDA underestimates the longwave CRE, especially in central Africa and northern South America. In the low latitude ocean, the δ-2DDA overestimates the longwave CRE (Fig. 8b). Outgoing longwave radiation at the TOA is mainly influenced by the temperature of the cloud top under the cloudy-sky condition. So the longwave CREs are related to the high cloud fraction. In Fig. 8d, the δ-4DDA enhances the longwave CRE compared to the δ-2DDA more significantly than that in the instantaneous diagnose experiment around the center of Africa, because of the more high cloud fraction simulated by δ-4DDA in the feedback test. In the Indian Ocean and the western Pacific warm pool, both the higher fraction of high cloud and effect of the calculation method itself cause the δ-4DDA to enhance the longwave CRE at TOA. In the instantaneous diagnose experiment, the δ-4DDA enhances the longwave CRE in the Atlantic and eastern Pacific. In the feedback experiment, the δ-4DDA reduces the CRE in these areas because of the decrease of high cloud fraction simulated by δ-4DDA.

Generally speaking, the performance of simulation results of CRE by δ-4DDA in the equatorial ocean region is poor. But the δ-4DDA produces more accurate shortwave CRE in the region over the land and ocean in the middle and high latitude areas. For

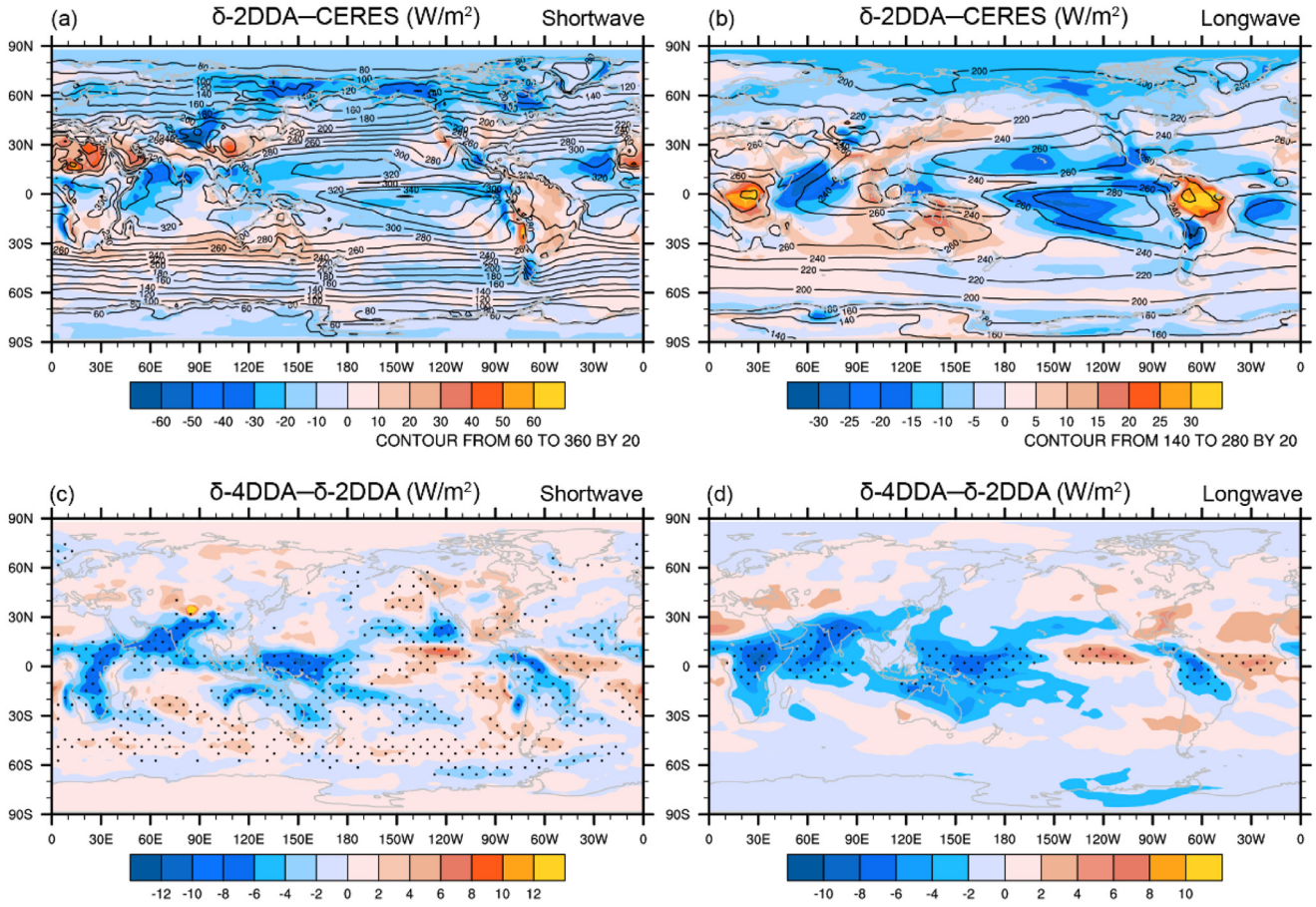

Fig. 7. Same as Fig. 6, but the net flux at TOA.

the longwave CRE, the simulation with δ-4DDA is better over the ground in Africa, South America, and Atlantic in the feedback experiment, all of which pass the reliability test.

The change of CREs must cause a change in heating rate. Fig. 9 shows the differences in the shortwave heating rate (Fig. 9a) and the longwave heating rate (Fig. 9b) between the two schemes in the feedback experiment. In general, in the feedback experiments, the shortwave heating rate at the tropospheric bottom is lower than the longwave heating rate. For shortwave heating rates, the differences between the two schemes are apparent throughout the troposphere. In the upper troposphere, the differences are more pronounced, especially at low latitudes, the maximum error is up to 0.069 K/day. The shortwave heating rate is closely related to aerosol absorption and other processes. In the lower troposphere, conditions such as aerosol and surface reflectance are more complex, making the differences of shortwave heating rate in the lower troposphere between two schemes more complicated than that in the upper layer. For the longwave heating rate, the large values of the differences between the two methods mainly appear in the lower troposphere. The longwave cooling simulated by δ-4DDA is strengthened near the tropopause but weakened in the troposphere. The longwave heating rate simulated by δ-4DDA scheme is significantly higher than that of the δ-2DDA in the middle and low latitudes, with a maximum difference of 0.59 K/day. This overestimation probably because the longwave CREs increase in the middle and low latitudes, which weakens the cooling effect of the longwave. The energy is concentrated below the clouds, increasing of the longwave heating rate.

Fig. 10a is the result of observed temperature from NCEP data and the difference between the simulated temperature by δ-2DDA and the NCEP data. The temperature of NCEP is generally zonal, decreasing from the equator to the poles. Compared with the NCEP, the δ-2DDA overestimates the heat over the ocean and underestimates the temperatures over the continents in the northern hemisphere and Antarctic. Fig. 10b presents the differences between δ-2DDA and δ-4DDA. In the middle latitudes and low latitudes, the temperature simulated by δ-4DDA is higher. The larger temperature differences were found in North America and Asia, where the maximum was 2.2 K. In the Antarctic, the temperature simulated by δ-4DDA is lower than that of δ-2DDA. At the bottom of the troposphere, the δ-4DDA simulates a higher heating rate in low and middle latitudes, which contributes to warmer temperatures in the middle and lower latitudes. In polar regions, the δ-4DDA heating rates are low, which may be the reason for the low temperature. The change in temperature is not the same as the change in heating rate, because the temperature can be modified not only by radiative heating but also by thermodynamic heating [66]. The temperature increases simulated by δ-4DDA of the northern and southern hemispheres at high latitudes are different, resulting in a larger temperature gradient in the southern hemisphere than in the northern hemisphere. The change in temperature gradient will affect large-scale circulation [[1], [33], [52]]. The temperature simulation of δ-2DDA in the land area of the northern hemisphere is lower than NCEP. The simulation of δ-4DDA in this area is better than that of δ-2DDA and pass the reliability test. In the region over the ocean, the δ-4DDA, like δ-2DDA, overestimates the temperature.

The δ-4DDA improves the humidity simulation compared to δ-2DDA, as shown in Fig. 11. Fig. 11a-b provides the results of specific humidity and Fig. 11c-d shows the results of relative humid-

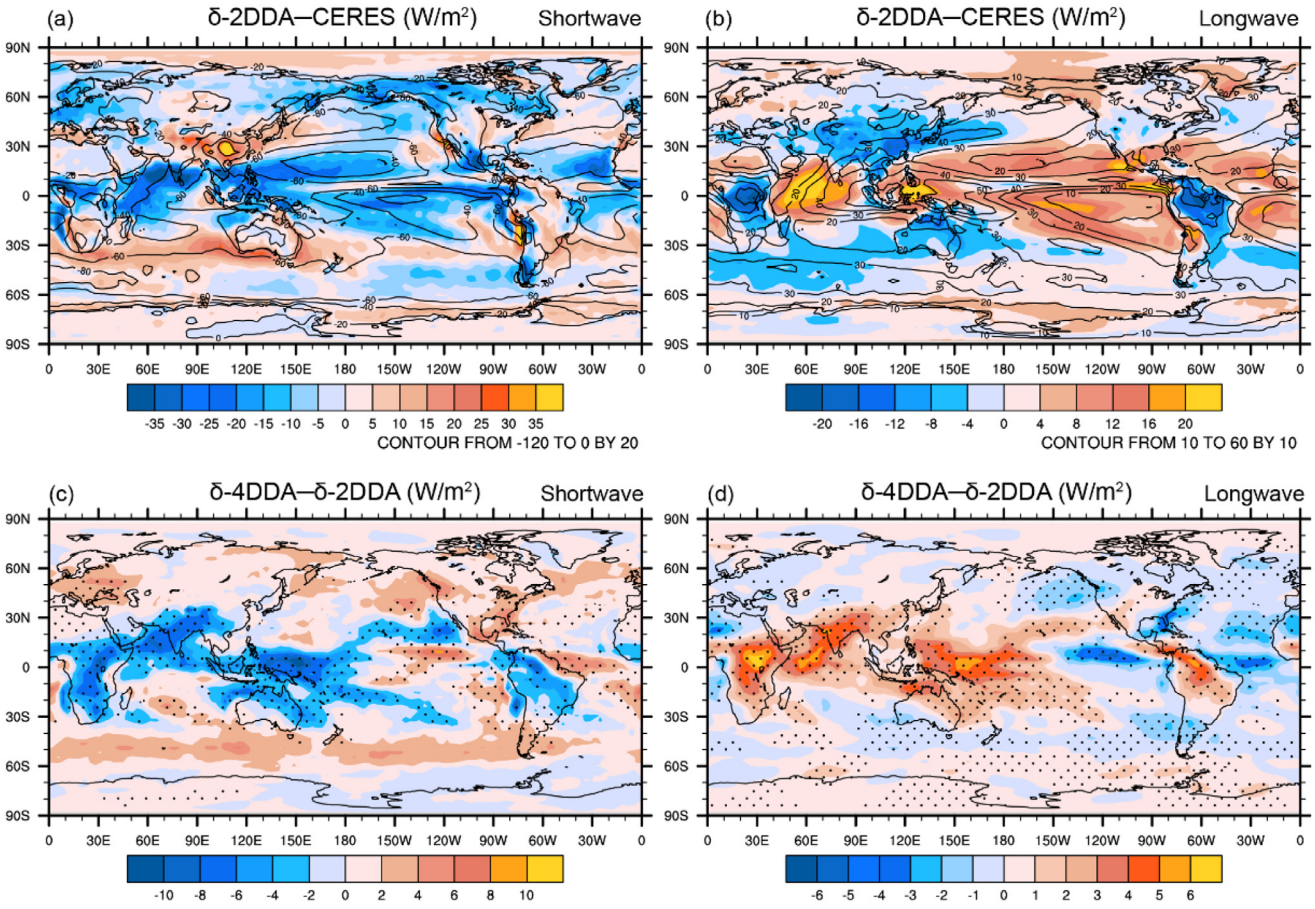

Fig. 8. Same as Fig. 6, but the CREs at TOA.

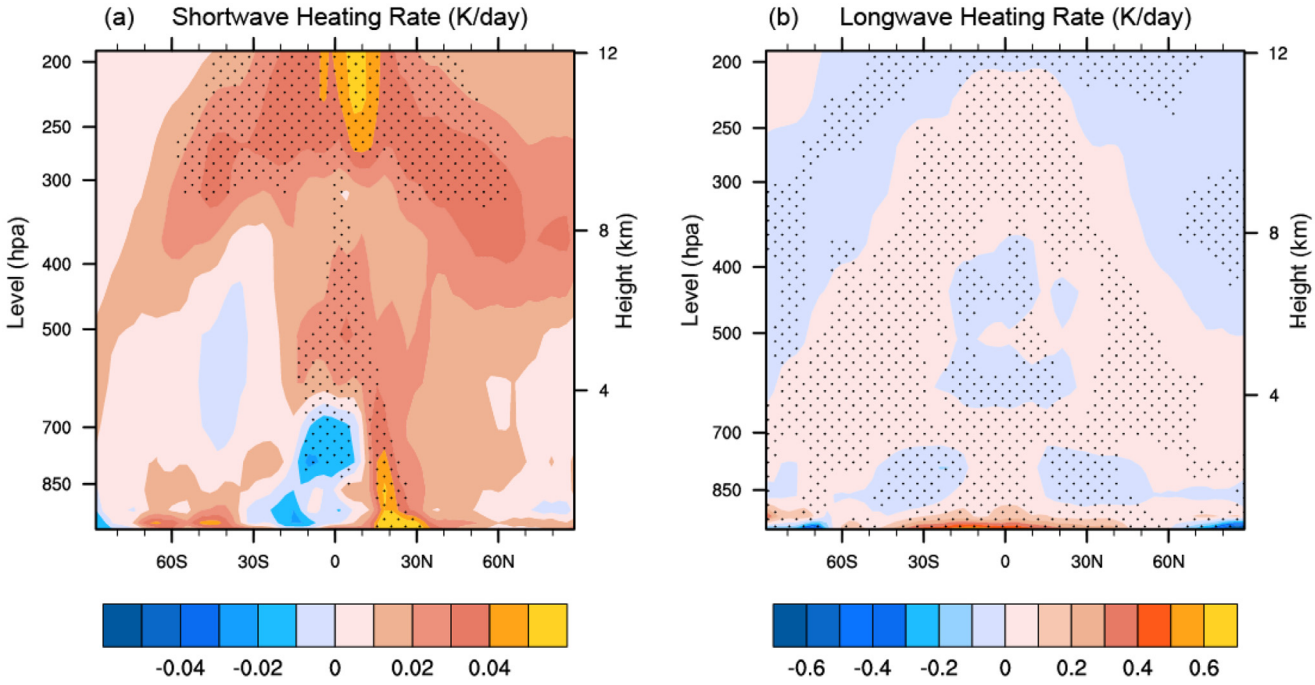

Fig. 9. Differences in heating rate in the troposphere between two schemes for (a) shortwave and (b) longwave in the feedback experiment. The black dots indicate where differences exceeded the 90% confidence level.

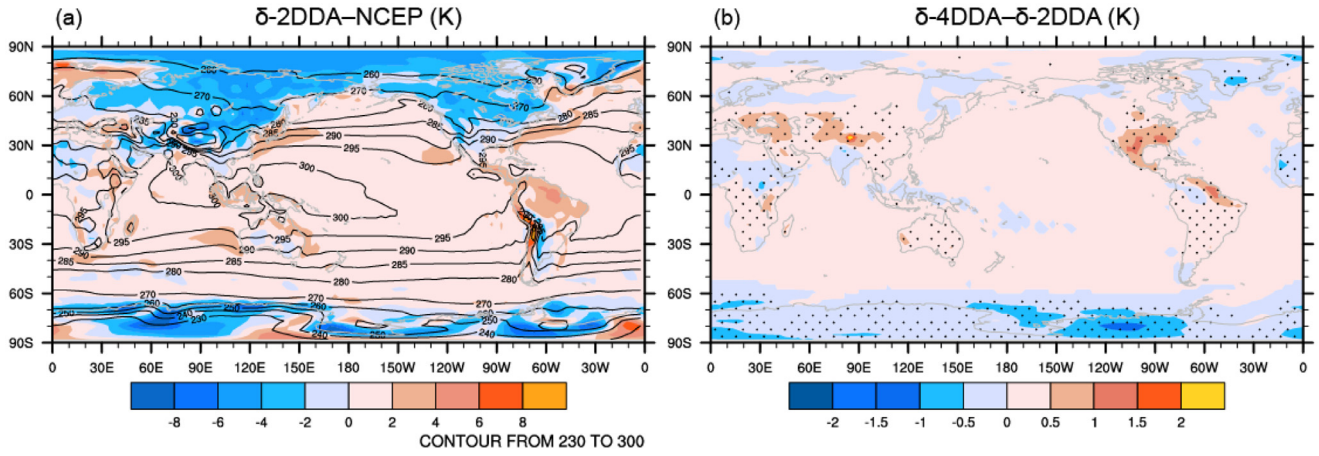

Fig. 10. Global distributions of differences in surface temperature (a) between δ-2DDA and NCEP, and (b) differences between two schemes in feedback experiment. The contours in (a) are the surface temperature of NCEP data. The black dots in (b) indicate where differences exceeded the 90% confidence level.

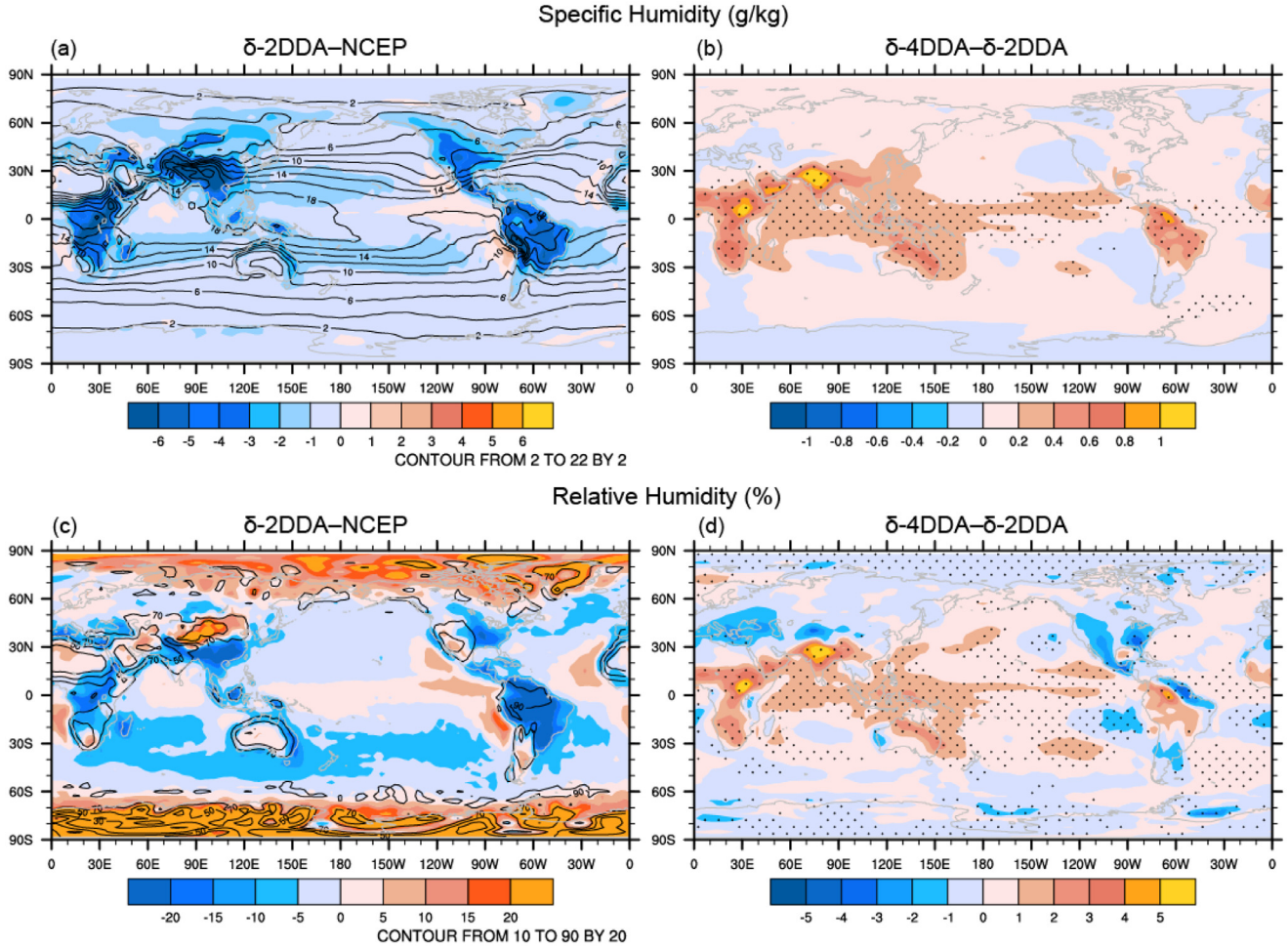

Fig. 11. Global distributions of differences in (a) specific humidity and (c) relative humidity between δ−2DDA and NCEP, and differences in (b) specific humidity and (d) relative humidity between two schemes in feedback experiment. The contours in (a) (c) are the humidity of NCEP data. The black dots in (b) (d) indicate where differences exceeded the 90% confidence level.

ity. The specific humidity of NCEP decreases from the equator to the poles. The relative humidity is higher in the ocean, lower in the Antarctic, Australia, the Sahara desert and the Arabian Peninsula. The δ-2DDA underestimates the specific humidity as a whole with significant errors appearing in the land at low and middle latitudes. Because the warmer environment can store more moisture, the specific humidity will increase with the increasing of temperature [22]. The specific humidity simulated by δ-4DDA is higher than that simulated by δ-2DDA except in the Antarctic region. The global average specific humidity error of δ-2DDA and δ-4DDA is −0.98 g/kg and −0.89 g/kg, respectively. In the low and middle latitudes, the improvement of specific humidity simulated

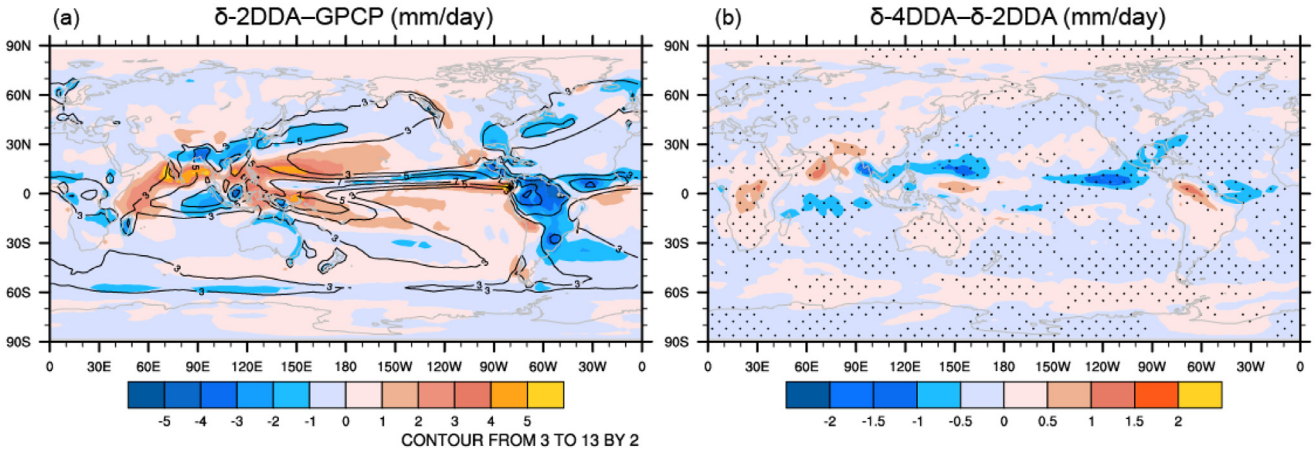

Fig. 12. Global distributions of differences in precipitation (a) between δ-2DDA and GPCP, and (b) differences between two schemes in feedback experiment. The contours in (a) are the precipitation of GPCP data. The black dots in (b) indicate where differences exceeded the 90% confidence level.

by δ-4DDA is more prominent. More water vapor warms the atmosphere through the greenhouse effect, which continues to increase water vapor through positive feedback [4,66]. The relative humidity is greatly overestimated by δ-2DDA in the Arctic and the Antarctic, which is different from the simulation of specific humidity. It may be related to the simulated low temperature in polar areas. In the equatorial ocean region, relative humidity simulated by δ-2DDA has a weak overestimation, while in other regions it is mostly underestimated. Compared with δ-2DDA, the δ-4DDA simulates lower relative humidity in polar regions and higher relative humidity in oceans and low-latitude lands. Overall, the simulation accuracy in specific humidity and relative humidity of δ-4DDA is higher than that of δ-2DDA.

Fig. 12 shows the simulation results in precipitation of the two schemes. High precipitation occurs in the regions at a low latitude ocean. The δ-2DDA underestimates precipitation in Africa and South America and significantly overestimates it in the northern Indian Ocean and western Pacific. From Fig. 10, the temperature gradient in the southern hemisphere simulated by the δ-4DDA increases, making the Hadley circulation in the south of hemisphere stronger ([1,33,52]). Affected by the enhanced Hadley circulation in the southern hemisphere, the intertropical convergence zone shifts northward [8,17,32], thus changing precipitation [56,66]. The precipitation simulated by the δ-4DDA in the equatorial region is generally less than that by the δ-2DDA. In some areas, precipitation increased, which may be related to increased water vapor [19]. Compared with the δ-2DDA, δ-4DDA simulates more precipitation in South America and Africa, with a maximum value of 1.46 mm/day. The simulated precipitation in the northern Indian Ocean and western Pacific is less, and the maximum difference is -2.21 mm/day, which means that δ-4DDA is more accurate in these areas than δ-2DDA. Generally speaking, precipitation simulated by δ-4DDA is more accurate than that of δ-2DDA in low latitudes. Also, simulations in precipitation of δ-4DDA over the ocean in the southern hemisphere, such as the South Pacific and ocean around the 60° south, are more accurate than that of δ-2DDA.

4. Conclusion and discussion

In this paper, both δ-2DDA and δ-4DDA radiation schemes are evaluated in GCM to compare the impact of different radiative transfer schemes, which helps us to choose the most suitable scheme for use in GCMs.

In the instantaneous diagnose experiment, in areas dominated by high clouds, the average difference in shortwave net flux at the surface and longwave net flux at the top of the atmosphere between δ-4DDA and δ-2DDA is more significant than that in the areas dominated by low clouds. The average difference in shortwave net flux at the top of the atmosphere is negative in the region dominated by high clouds, while positive in areas dominated by low clouds. The δ-4DDA reduces the negative shortwave CRE in the areas with the large fraction of low cloud, while it enhances the negative shortwave CRE in the areas with the large fraction of high cloud compared to the δ-2DDA. For the longwave CRE, the δ-4DDA enhances the longwave CRE drastically in the areas with a large fraction of the high cloud. Generally speaking, the δ-4DDA reduces the shortwave CRE errors over the land and ocean in the middle and high latitudes and reduces the longwave CRE errors over the land. But over the ocean in low latitudes, δ-2DDA performs better both for shortwave CRE and longwave CRE. In a feedback experiment, the fluxes and CRE changes from the combined impact of the distribution of cloud and the calculation method. δ-4DDA produces more accurate shortwave CRE in the part of the land and ocean in the middle and high latitude areas. The differences in the fractions of high cloud influence the longwave CRE at TOA observably. The longwave CRE simulated by δ-4DDA is better over the land in Africa, South America, and Atlantic. The δ-4DDA simulates more accurate temperature in continents of the northern hemisphere and precipitation in North America, Africa, north of Indian Ocean, and western Pacific. For specific humidity and relative humidity, the δ-4DDA simulations are better than δ-2DDA around the world.

In this paper, we choose the data from CERES, NCEP, and GPCP as the benchmark to evaluate the two schemes. We chose these data because the datasets are accessible and they provide the variables we want to compare. These data are also widely used in GCM community as a criterion [10,14,35,37]. However, the comparability of these data and model simulation data needs to be further explored, as the external forcing of the two types of data are not completely consistent. How to compare with these two data is an interesting and challenging problem and has not been done so far.

From previous studies [57,59], the δ-4DDA is more superior to δ-2DDA, especially under the cloudy-sky condition. Improvements in the accuracy of radiation modules are necessary, which directly affect other physical processes such as temperature, humidity, and precipitation. Therefore implementing δ-4DDA scheme into GCM and evaluating its performance is meaningful. However, the δ-4DDA scheme will result in the worse performance of GCM in some areas compared with δ-2DDA, since errors produced by the δ-2DDA may be offset by those provided by other inaccurate physical parameterization. Therefore, other physical processes in GCMs, such as the cloud microphysics process, should also be im-

proved meanwhile for the better performance of GCMs when using more accurate radiative schemes.

Author_Statment

We greatly appreciate the comments from you and the reviewers on our manuscript entitled "Impact of δ-Four-Stream Radiative Transfer Scheme on Global Climate Model Simulation". We have studied reviewer's comments carefully and revised our manuscript. All authors agree to this change. We would like to express our great appreciation to you and reviewers for comments on our paper. Looking forward to hearing from you. Thank you so much for your kind support.

Declaration of Competing Interest

None.

Acknowledgments

We thank the National Climate Center for providing BCC_AGCM model. This work was supported by the National Key R&D Program of China (2018YFC1507002), the National Natural Science Foundation of China (41675003 and 41675056) and Postgraduate Research & Practice Innovation Program of Jiangsu Province.

References

[1] Adam O, Schneider T, Harnik N. Role of changes in mean temperatures versus temperature gradients in the recent widening of the Hadley circulation. J Clim 2014;27:7450–61.
[2] Ayash T, Gong S, Jia CQ. Implementing the delta-four-stream approximation for solar radiation computations in an atmosphere general circulation model. J Atmos Sci 2008;65(7):2448–57.
[3] Chou MD. A solar radiation model for use in climate studies. J Atmos Sci 1992;49(9):762–72.
[4] Ceppi P, Shepherd T. Contributions of climate feed-backs to changes in atmospheric circulation. J Clim 2017;30:9097–118.
[5] Chandrasekhar S. Radiative transfer. Oxford University Press; 1950. p. 393.
[6] Colman R. A comparison of climate feedbacks in general circulation models. Clim Dyn 2003;20(7):865–73.
[7] Curry JA, Webster PJ. Climate science and the uncertainty monster. Bull Am Meteor Soc 2011;92(12):1667–82.
[8] Dargan MDF, Hwang YT. Extratropical influence on ITCZ shifts in slab ocean simulations of global warming. J Clim 2011;25:720–33.
[9] Doicu A, Efremenko D, Trautmann T. A multi-dimensional vector spherical harmonics discrete ordinate method for atmospheric radiative transfer. J Quant Spectrosc Radiat Transfer 2013;118:121–31.
[10] Dolinar EK, Dong X, Xi B, Jiang JH, Su H. Evaluation of CMIP5 simulated clouds and TOA radiation budgets using NASA satellite observations. Clim Dyn 2015;44(7–8):2229–47.
[11] Dong X, Xi B, Minnis P. A climatology of midlatitude continental clouds from the ARM SGP central facility. Part II: cloud fraction and surface radiative forcing. J Clim 2006;19(9):1765–83.
[12] Eastman R, Warren SG, Hahn CJ. Variations in cloud cover and cloud types over the ocean from surface observations, 1954-2008. J Clim 2011;24:5914–34.
[13] Efremenko D, Doicu A, Loyola D, Trautmann T. Small-angle modification of the radiative transfer equation for a pseudo-spherical atmosphere. J Quant Spectrosc Radiat Transfer 2013;114:82–90.
[14] Forster PMcoauthors. Evaluation of radiation scheme performance within chemistry climate models. J Geophys Res 2011;116:D10302.
[15] Fu Q, Liou KN, Cribb MC, Charlock TP, Grossman A. Multiple scattering parameterization in thermal infrared radiative transfer. J Atmos Sci 1997;54(24):2799–812.
[16] Gu Y, Fararra J, Liou KN, Mechoso CR. Parameterization of cloud-radiation processes in the UCLA general circulation model. J Clim 2003;16(20):3357–70.
[17] Hawcroft M, Haywood JM, Collins M, Jones A, Jones AC, Stephens G. Southern ocean albedo, inter-hemispheric energy transports and the double ITCZ: global impacts of biases in a coupled model. Clim Dyn 2016;48:2279–95.
[18] Hill PG, Manners J, Petch JC. Reducing noise associated with the monte carlo independent column approximation for weather forecasting models. Quart J R Meteor Soc 2011;137:219–28.
[19] Holton J. An introduction to dynamic meteorology. Academic Press; 2004. p. 372.
[20] Hu S, Gao T-C, Li H, et al. Effect of atmospheric refraction on radiative transfer in visible and near-infrared band: model development, validation, and applications. J Geophys Res Atmos 2016:121. doi:10.1002/2015JD024105.
[21] Jing XW, Zhang H. Application and evaluation of MCICA cloud-radiation framework in the AGCM of the national climate center. Chin J Atmos Sci (in Chinese) 2012;36(5):945–58.
[22] Kang SM, Seager R, Frierson DMW, Liu X. Croll revisited: why is the northern hemisphere warmer than the southern hemisphere? Clim Dyn 2015;44:1457–72.
[23] Kiehl JT, Hack JJ, Briegleb BP. The simulated earth radiation budget of the national center for atmospheric research community climate model CCM2 and comparisons with the earth radiation budget experiment (ERBE). J Geophys Res 1994;99(D10):20815–27.
[24] Kylling A, Stamnes K, Tsay SC. A reliable and efficient two-stream algorithm for spherical radiative rransfer: documentation of accuracy in realistic layered media. J Atmos Chem 1995;21:115–50.
[25] Li J, Ramaswamy V. Four-stream spherical harmonic expansion approximation for solar radiative transfer. J Atmos Sci 1996;53(8):1174–86.
[26] Li J, Dobbie JS. Four-stream isosector approximation for solar radiative transfer. J Atmos Sci 1998;55(4):558–67.
[27] Li J, Barker HW. A radiation algorithm with correlated-k distribution. Part I: local thermal equilibrium. J Atmos Sci 2005;62(2):286–309.
[28] Lin H, Zhang F, Wu K, Xu J. Comparisons of δ-two-stream and δ-four-stream radiative transfer schemes in RRTMG for solar spectra. Sci Online Lett Atmos 2019;15:87–93.
[29] Liou KN. Analytic two-stream and four-stream solutions for radiative transfer. J Atmos Sci 1974;31:1473–5.
[30] Liou KN, Fu Q, Ackerman TP. A simple formulation of the delta–four-stream approximation for radiative transfer parameterizations. J Atmos Sci 1988;45(13):1940–7.
[31] Liou KN. An introduction to atmospheric radiation. San Diego: Academy Press; 2002. p. 499.
[32] Loeb NG, Wang H, Cheng A, Kato S, Fasullo JT, Xu KM, et al. Observational constraints on atmospheric and oceanic cross-equatorial heat transports: revisiting the precipitation asymmetry problem in climate models. Clim Dyn 2016;46:3239–57.
[33] Lu J, Vecchi GA, Reichler T. Expansion of the Hadley cell under global warming. Geophys Res Lett 2007;34:L06805.
[34] Lu P, Zhang H, Li J. A comparison of two-stream disort and eddington radiative transfer schemes in a real atmospheric profile. J Quant Spectrosc Radiat Transfer 2009;110(1–2):129–38.
[35] Lucio PS. Assessing HadCM3 simulations from NCEP reanalyses over Europe: diagnostics of block-seasonal extreme temperature's regimes. Global Planet Change 2004;44(1–4):0–57.
[36] Minnis P, Young DF, Wielicki BA, Sun-Mack S, Trepte QZ, Chen Y, Heck PW, Dong X. A global cloud database from VIRS and MODIS for CERES. In: *Proc. SPIE 4891, Optical Remote Sensing of the Atmosphere and Clouds III*; 2003. p. 115–26.
[37] Nabat P, Somot S, Mallet M, Sevault F, Chiacchio M, Wild M. Direct and semi-direct aerosol radiative effect on the mediterranean climate variability using a coupled regional climate system model. Clim Dyn 2015;44(3–4):1127–55.
[38] Nakajima T, Tsukamoto M, Tsushima Y, Numaguti A, Kimura T. Modeling of the radiative process in an atmospheric general circulation model. Appl Opt 2000;39:4869–78.
[39] Oreopoulos Lcoauthors. The continual intercomparison of radiation codes: results from phase I. J Geophys Res 2012;117:D06118.
[40] Pincus R, Barker HW, Morcrette JJ. A fast, flexible, approximate technique for computing radiative transfer in inhomogeneous cloud fields. J Geophys Res 2003;108(D13):4376.
[41] Ramanathan V, Cess RD, Harrison EF, Minnis P, Barkstrom BR, Ahmad E, et al. Cloud-radiative forcing and climate: results from the earth radiation budget experiment. Science 1989;243(4887):57–63.
[42] Saito M, Iwabuchi H. Cloud discrimination from sky images using a clear sky index. J Atmos Ocean Technol 2016;33:1583–95.
[43] Salgueiro V, Costa MJ, Silva AM, Bortoli D. Variability of the daily-mean shortwave cloud radiative forcing at the surface at a mid-latitude site in southwestern Europe. J Clim 2014;27(20):7769–80.
[44] Yining S, Zhang F, Chan KL, Li W, Lin H, Duan M. An improved Eddington approximation method for irradiance calculation in a vertical inhomogeneous medium. J Quant Spectrosc Radiative Transfer 2019;226:40–50.
[45] Soden BJ, Held IM. An assessment of climate feedbacks in coupled ocean atmosphere models. J Clim 2006;19(14):3354–60.
[46] Stephens GL. Cloud feedbacks in the climate system: a critical review. J Clim 2005;18(2):237–73.
[47] Sun B, Kattawar GW, Yang P, Mlawer E. An improved small-angle approximation for forward scattering and its use in a fast two-component radiative transfer method. J Atmos Sci 2017;74:1959–87.
[48] Sun Z, Rikus L. Improved application of exponential sum fitting transmissions to inhomogeneous atmosphere. J Geophys Res 1999;104(D6):6291–303.
[49] Sun Z, Liu A. Fast scheme for estimation of instantaneous direct solar irradiance at the Earth's surface. Solar Energy 2013;98:125–37.
[50] Tian W, Chiu WKS. A two-dimensional scheme for axisymmetric radiative heat transfer using the finite-volume method. Numer Heat Tr B Fund 2005;47(3):199–211.
[51] Williams KD, Tselioudis G. GCM intercomparison of global cloud regimes: present-day evaluation and climate change response. Clim Dyn 2007;29(2–3):231–50.
[52] Wu K, Li J, Cole J, Huang X, Salzen KV, Zhang F. Accounting for seveval infrared radiation processes in climate model. J Clim 2019;32:4601–20.

[53] Wu T, Yu R, Zhang F, Wang Z, Dong M, Wang L. The Beijing climate center atmospheric general circulation model: description and its performance for the present-day climate. Clim Dyn 2010;34:123–47.
[54] Xu J, Schreier F, Doicu A, Trautmann T. Assessment of Tikhonov-Type regularization methods for solving atmospheric inverse problems. J Quant Spectrosc Radiat Transfer 2016;184:274–86.
[55] Yang Q, Zhang F, Zhang H, Wang Z, Li J, Wu K, et al. Assessment of two-stream approximations in a climate model. J Quant Spectrosc Radiat Transfer 2019;225:25–34.
[56] Zăgar N, Skok G, Tribbia J. Climatology of the ITCZ derived from ERA interim reanalyses. J Geophys Res Atmos 2011;116:D15103.
[57] Zhang F, Shen Z, Li J, Zhou X, Ma L. Analytical delta-four-stream doubling-adding method for radiative transfer parameterizations. J Atmos Sci 2013;70(3):794–808.
[58] Zhang F, Li J. Doubling-adding method for delta-four-stream spherical harmonic expansion approximation in radiative transfer parameterization. J Atmos Sci 2013;70(10):3084–101.
[59] Zhang F, Wu K, Li J, Yang Q, Zhao J, Li J. Analytical infrared delta-four-stream adding method from invariance principle. J. Atmos. Sci. 2016;73(10):4171–88.
[60] Zhang H, Nakajima T, Shi G, Suzuki T, Imasu R. An optimal approach to overlapping bands with correlated K-distribution method and its application to radiative calculations. J Geophys Res 2003;108(D20):4641.
[61] Zhang H, Shi G, Nakajima T, Suzuki T. The effects of the choice of the K-interval number on radiative calculations. J Quant Spectrosc Radiat Transfer 2006;98:31–43.
[62] Zhang H, Suzuki T, Nakajima T, Shi G, Zhang X, Liu Y. Effects of band division on radiative calculations. Optical Engineering 2006;45(1):016002.
[63] Zhang H, Jing XW, Li J. Application and evaluation of a new radiation code under MCICA scheme in BCC_AGCM2.0.1. Geosci Model Dev 2014;7:737–54.
[64] Zhang H, Wang Z, Zhang F, Jing X. Impact of four-stream radiative transfer algorithm on aerosol direct radiative effect and forcing. Int J Climatol 2015;35:4318–28.
[65] Zhang H, Chen Q, Xie B. A new parameterization for ice cloud optical properties used in BCC-RAD and its radiative impact. J Quant Spectrosc Radiat Transfer 2015;150:76–86.
[66] Zhao W, Peng Y, Wang B, Li J. Cloud longwave scattering effect and its impact on climate simulation. Atmosphere 2018;9:153.